HHS Public Access

Author manuscript

Arthritis Rheumatol. Author manuscript; available in PMC 2024 August 21.

Published in final edited form as:

Arthritis Rheumatol. 2022 December ; 74(12): 1971–1983. doi:10.1002/art.42284.

Modulation of the itaconate pathway attenuates murine lupus

Luz P. Blanco, Ph.D.[1], **Eduardo Patino-Martinez, Ph.D.**[1], **Shuichiro Nakabo, M.D., Ph.D.**[1], **Mingzeng Zhang, M.D., Ph.D.**[1], **Hege L. Pedersen, Ph.D.**[1,*], **Xinghao Wang, B.S.**[1], **Carmelo Carmona Rivera, Ph.D.**[1], **Dillon Claybaugh, B.S.**[1], **Zu-Xi Yu, M.D.**[2], **Equar Desta, B.S.**[3], **Mariana J. Kaplan, M.D.**[1]

[1]Systemic Autoimmunity Branch, National Institute of Arthritis and Musculoskeletal and Skin Diseases (NIAMS)

[2]Pathology Core, National Heart, Lung, and Blood Institute (NHLBI)

[3]Laboratory of Animal Science Section, National Institute of Allergy and Infectious Diseases (NIAID), National Institutes of Health (NIH), Bethesda, Maryland, USA.

Abstract

Background: Itaconic acid, a Kreb's cycle derived immunometabolite, is synthesized by myeloid cells in response to danger signals to control inflammasome activation, type I Interferon (IFN) responses and oxidative stress. As these pathways are dysregulated in systemic lupus erythematosus (SLE), we investigated the role of an itaconic acid derivative in the treatment of established murine lupus.

Methods: Female New Zealand Black/New Zealand White F1 lupus prone mice were administered 4-octyl itaconate (4-OI) or vehicle starting after clinical onset of disease (30 weeks of age) for 4 weeks (n=10 mice /group). At 34 weeks of age (peak disease activity) animals were euthanized, organs and serum collected, and clinical, metabolic, and immunologic parameters were evaluated.

Results: Proteinuria, kidney immune complex deposition, renal scores of severity and inflammation and anti-RNP autoantibodies were significantly reduced in 4-OI treatment group compared to vehicle. Splenomegaly decreased in 4-OI group compared to vehicle, with decreases in activation markers in innate and adaptive immunes cells, increases in $CD8^+$ T cell numbers and inhibition of JAK1 activation. Gene expression analysis in splenocytes showed significant decreases in type-I IFN and proinflammatory cytokine genes and increased Treg associated markers in the 4-OI group when compared to vehicle. In human control and lupus myeloid cells, 4-OI in vitro treatment decreased proinflammatory responses and B cell responses.

Correspondence and reprint requests: Mariana J. Kaplan, M.D., Systemic Autoimmunity Branch, NIAMS/NIH, 10 Center Drive; 12N248C, Bethesda, MD 20892, mariana.kaplan@nih.gov.

*Current address: RNA and Molecular Pathology Research Group, Department of Medical Biology, Faculty of Health Sciences, UTI The Artic University of Norway, Tromsø, Norway, and Center for Clinical Research and Education University Hospital of North Norway, Tromsø, Norway.

Author contributions

LPB and MJK conceived the study, designed experiments, and wrote the manuscript. LPB, EPM, SN, MZ, HLP, XW, CC-R, DC, and DE performed experiments; ZXY performed histopathologic analysis; LPB analyzed the data and generated the graphs and stats shown in this work.

There are no conflicts of interest.

Conclusions: These results support targeting immunometabolism as a potentially viable approach in autoimmune diseases treatment, with 4-OI displaying beneficial roles attenuating immune dysregulation and organ damage in lupus.

Introduction

Systemic lupus erythematous (SLE) is a complex autoimmune syndrome in which multi-organ damage leads to enhanced morbidity and mortality (1, 2). Many individuals affected by SLE require immunosuppression and there is need for additional effective immunomodulatory drugs with less side effects (3).

Among some of the innate immune abnormalities characteristic of SLE, dysregulated type I Interferon (IFN) responses, inflammasome activation, and enhanced oxidative stress are prevalent (4, 5). In addition, our group and others have described a role for mitochondrial dysfunction in SLE pathogenesis (6–9). Itaconic acid is a mitochondrial-derived immune-metabolite that modulates several of these dysregulated pathways (10). Itaconic acid is synthesized by macrophages following lipopolysaccharide (LPS) challenge and, more broadly, in cells expressing the aconitate decarboxylase 1 (*ACOD1*) gene (also known as *IRG1*). This gene codifies for an enzyme which acts via decarboxylation of cis-aconitate to produce itaconic acid from the tricarboxylic acid cycle in response to proinflammatory stimuli (11). Itaconic acid effects are broad and pleiotropic, modulating not only metabolism but also inflammatory and oxidative stress-related responses (12).

Because of these anti-inflammatory activities, itaconic acid improved derivatives have been isolated. In particular, 4-octyl itaconate (4-OI) is a cell-soluble electrophilic small molecule that alkylates proteins and inhibits inflammasome activation (10). Among several key targets for alkylation are Keap1 and Gapdh, whose modifications lead to activation of the Nrf2 transcription factor and inhibition of aerobic glycolysis, respectively (13, 14). As such, Nrf2 is considered a master regulator of cellular anti-oxidative and detoxification responses, while Gapdh inhibition reduces the aerobic glycolysis or Warburg effect that predominate in activated immune cells under inflammatory conditions. Furthermore, Nrf2 activation by 4-OI downregulates type I IFN synthesis by the c-GAS-STING pathway (15). In some *in vivo* animal models 4-OI can attenuate tissue injury by reducing inflammation and oxidative stress (16–21). Moreover, the 4-OI-Nrf2 anti-inflammatory axis effectively reduces proinflammatory cytokine expression *in vitro* in SLE PBMCs (22). Given these observations, we assessed whether therapy with 4-OI would ameliorate clinical and immunologic parameters of established murine lupus.

Materials and Methods.

Animals and *in vivo* treatment:

Female NZBWF1/J (NZB/W stock #100008) mice were purchased from The Jackson Laboratories (Bar Harbor, ME). NIAMS Animal Care and Use Committee approved animal procedures (protocol #A019–05-03) without randomization and all researchers were unblinded (at least 4 mice/cage). NZB/W mice received subcutaneous 4-OI (14 ug/kg/min; Cayman Chemical, #25374, Ann Arbor, MI) or vehicle control (2-hydroxypropyl-beta

cyclodextrin 40% (SIGMA Aldrich, #332607, St Louis, MO) in PBS via osmotic pump delivery (Alzet, #2006, Cupertino, CA), surgically inserted in the dorsum of the animals at 30 weeks old (n=9/group). Number, age, and sex of animals were determined based on our previous experimental designs that showed that 9–10 female lupus-prone mice/group provided sufficient power when comparing various active treatments versus controls. At 34 weeks of age (expected peak disease activity), mice were euthanized, and tissues and blood collected for analysis.

Complete blood count:

This was performed in the NIH Department of Laboratory Medicine using murine blood diluted 1:3 in PBS with an Advia 120 device.

Splenocyte gene expression:

mRNA was purified from frozen spleens in RNA-later, stored at −80°C and quantification of proinflammatory mRNAs was performed as described (23, 24). Briefly, tissue was homogenized in RLT lysis buffer and RNA isolated with RNA Easy kit (QIAGEN); cDNA was synthesized using 1 ug of RNA, BIORAD iScript kit, and an ABI thermocycler. RT PCR was performed using BIORAD reagents and instructions, and a CFX96 BIORAD real time thermocycler. Fold gene expression for each gene was calculated using *B2m* as house-keeping gene and Ct from mouse tissue for the 4-OI or control vehicle conditions for delta delta calculations. The following primers were used: *Ifna1* (forward: 5'- AAG GAC AGG CAG GAC TTT GGA TTC −3′, reverse: 5′- GAT CTC GCA GCA CAG GGA TGG −3′); *Ifnb* (forward: 5′- AAG AGT TAC ACT GCC TTT GCC ATC −3′, reverse: 5′- CAC TGT CTG CTG GTG GAG TTC ATC −3′); *Il6* (forward: 5′- TGG CTA AGG ACC AAG ACC ATC CAA −3′, reverse: 5′- AAC GCA CTA GGT TTG CCG AGT AGA −3′); *Tnf* (forward: 5′- CCC TCA CAC TCA GAT CAT CTT CT −3′, reverse: 5′- GCT ACG ACG TGG GCT ACA G −3′); *Il1b* (forward: 5′- CCC TGC AGC TGG AGA GTG TGG A −3′, reverse: 5′- CTG AGC GAC CTG TCT TGG CCG −3'); *Ebi3* (forward: 5'- GTT CTC CAC GGT GCC CTA C −3', reverse: 5'- CGG CTT GAT GAT TCG CTC −3'); *Il12a* (forward: 5'- CCA CCC TTG CCC TCC TAA A −3', reverse: 5'- GCC GTC TTC ACC ATG TCA TCT −3'); *Foxp3* (forward: 5'- CTG CCT TGG TAC ATT CGT GA −3', reverse: 5'- CCA GAT GTT GTG GGT GAG TG −3'); *Ikzf2* (forward: 5'- TAA GCT CAG CTT ATT CTC AGG TCT ATCA −3', reverse: 5'- ATG TTG TTT TCG TGA CTA TCA GAT GTT −3'); *p40* (forward: 5'- CGT GCA CTG AGG CTC AGA AAT GTT TC −3', reverse: 5'- TTT CTT TGC ACC AGC CAT GAG C −3'). Mitochondrial/nuclear splenocyte transcription ratio was calculated using the following primers: *16S* or *Mrnr2* (forward: 5′- CTA GAA ACC CCG AAA CCA AA −3′, reverse: 5′- CCA GCT ATC ACC AAG CTC GT −3′) and beta-2-microglobulin *B2m* also used as housekeeping gene (forward: 5′- ATG GGA AGC CGA ACA TAC TG −3′, reverse: 5′- CAG TCT CAG TGG GGG TGA AT −3′). All the primers were purchased from IDT Integrated DNA Technologies (Coralville, IA).

Splenocyte immunophenotyping by flow cytometry:

Splenocytes (1×10^6) were suspended in 100 ul of FACS buffer, incubated with 1ul of TruStain FcX (BioLegend, catalog #422302, San Diego CA), at 4°C for 15 minutes, followed by incubation with various fluorochrome-conjugated antibodies (all

from BioLegend) at 4°C for 30 minutes. Cells were washed twice and immediately analyzed on a BD FACS Celesta flow cytometer (BD Biosciences, Franklin Lakes, NJ) followed by FlowJo software. The following anti-mouse, fluorochrome labeled-antibodies were used: **panel 1:** APC_CD86 (#105012), APC-Cy7_CD11b (#101226), BV421_CD19 (#124608), PE_CD80 (#104708), PE-Cy7_CD11c (#117318), Percp-Cy5.5_MHCII (#116416); **panel: 2** APC_Ly-6C (#128016), APC-Cy7_CD86 (#105030), BV421_Ly-6G (#127628), FITC_CD40 (#124608), PE_CD11b (#101208), PE-Cy7_CD45 (#103114), Perp-Cy5.5_MHCII (#116416); **panel 3:** APC_CD23 (#101620), APC-Cy7_CD21 (#123418), BV421_CD19 (#115538), FITC_CD45 (#103108), PE_IgD (#405706), PE-Cy7_IgM (#406514), Percp-Cy5.5_CD138 (#142510); **panel 4:** APC_CD8 (#100712), APC-Cy7_CD44 (#103028), BV421_CD4 (#100438), FITC_CD19 (#115506), PE_CD62L (#104408), PE-Cy7_CD3 (#100220), Percp-Cy5.5_CD45 (#103132); **panel 5:** APC_CD11c (#117310), PB_B220 (#103227), FITC_CD45 (#103108), PE_PDCA-1 (#127104).

JAK1 activation in splenocytes:

JAK1 activation was quantified by dual ELISA to detect phosphorylated and total JAK1 simultaneously in splenic tissue samples preserved at −80°C and lysed using manufacturer's instructions (RayBiotech, #PEL-JAK1-Y1022-T-1, Peachtree Corners, GA). Spleen lysates contained 753 ug/ml protein. OD 450 nm was measured using FLUOstar Omega BMG Labtech (Cary, NC) plate reader.

Endothelium-dependent vasorelaxation:

Vasorelaxation assessments of murine aortic rings were performed as described (25), with reagents purchased from SIGMA-Aldrich. Briefly, aortic rings (~2 mm) were excised and maintained in physiological salt solution (PSS) with aeration (95% O_2 /5% CO_2). After equilibration for 1 hour, contraction was achieved with PSS containing 100 mM potassium chloride. Relaxed aortic rings were contracted with phenylephrine. Vasorelaxation was assessed by addition of a gradient of acetylcholine ($1 \times 10{-}9$ M to $1 \times 10{-}5$ M). Results were reported as percentage of phenylephrine contraction.

Kidney histology analysis and immune complex (IC) deposition quantification.

Kidney slides were evaluated blindly by a veterinary pathologist for scoring of glomerular, tubulointerstitial, vascular and lymphoproliferative lesions, as described (26). Histology evaluations were made from paraffin embedded slides with H&E, Masson tri-chrome and PAS staining by semiquantitative analysis (0, no changes; 1, mild changes; 2, moderate changes and 3 severe changes).

Renal IC deposition was quantified as described (23) using Alexa fluor 594-F(ab')2-goat anti-mouse IgG (Thermo Fisher, #A11020, Waltham, MA) and FITC-anti-murine C3 antibody (Immunology Consultants Laboratories, #GC3–90F-Z, Portland, OR). Three random images were obtained from each stained frozen section, which were analyzed with Image J software, selecting the glomerular compartment to quantify mean pixels for each fluorescence channel used.

Quantification of serum autoantibodies:

Serum anti-dsDNA and anti-RNP quantification was performed as described (23) using commercially available ELISA kits (#5110, #5410, Alpha Diagnostic International, San Antonio, TX, respectively). Serum samples were diluted 1:125 in the low NSB buffer and the assay was performed following manufacturer's instructions.

Proteinuria determination:

Urine albumin:creatinine ratio was determined as described (23) using ELISA kits for creatinine and mouse albumin (Exocell, #1012 and 1011 respectively, Philadelphia, PA), following t manufacturer's instructions.

Bone marrow (BM) isolation and differentiation of murine macrophages:

NZB/W BM precursors were treated *in vivo* with 4-OI or vehicle, purified and cultured for 24 hours in DMEM (Gibco, #11995–065, Thermo Fisher), supplemented with 10 % FBS and 1 % Penicillin-Streptomycin. After 24 hours, medium was replaced, and BM-derived macrophages (BMDM) were cultured (1.0×10^6 cells/ml) in 96-well Seahorse plates for 6 days in DMEM medium containing M-CSF 50 ng/mL (R&D Systems, #216-MC, Minneapolis, MN). M-CSF was replaced every two days.

Quantification of NETs and mitochondrial ROS (mROS):

Isolation of mouse BM- derived neutrophils and human peripheral blood neutrophils, quantification of NET formation, and mROS were performed as described by us (23). Briefly, BM neutrophils were purified with Percoll gradient and human neutrophils using sedimentation with 2% Dextran, following a Ficoll gradient. Cells were seeded in 96-well plates (200,000 cells/ 100 ul/ well in triplicates for each dye) and allowed to form NETs in the presence of SYTOX (to quantify extracellular DNA, 1 uM final concentration), Quant-It Picogreen (to quantify total DNA; stock solution diluted 1:250) and MitoSox (to quantify mROS; final concentration 200 ng/ml). All dyes were from Thermo Fisher. At baseline, 1 or 2 hours, fluorescence was measured for Picogreen (485/520), Mitosox (510/580), and SYTOX (485/520), respectively using a FLUOstar Omega BMG Labtech (Cary, NC) plate reader. Cells without dye were used as blank.

Seahorse analysis:

This was performed as described (27). The following reagents (Sigma Aldrich) were used: glucose (#G8769), oligomycin (#75351), carbonyl cyanide-4-(trifluoro-methoxy) phenylhydrazone (FCCP, #C2910), 2-deoxy-d-glucose (2-DG, #D1634), rotenone (#R8875), antimycin A (#A8674), and sodium pyruvate (#S8636). L-glutamine (#103579–100), XF calibrant (pH 7.4, #10084–000), XF RPMI medium (pH 7.4, #103576–100). Seahorse plates and cartridges were from Agilent (Santa Clara, CA). BM- derived macrophages or splenocytes were plated on Corning Cell-Tak -coated Seahorse culture plates (300,000 cells/well, Thermo Fisher Scientific, #354240) in XF RPMI medium (pH 7.4). Seahorse XF analysis was performed at 37°C with no CO_2, using the XF-96e analyzer (Agilent), following manufacturer's instructions. Mitochondrial stress test assay was performed using Seahorse XF RPMI medium with 25 mM glucose, 1 mM sodium pyruvate, and 2 mM

L-glutamine. For mitochondrial stress tests, cells were treated serially with oligomycin (5 μM), FCCP (1 μM), rotenone (100 nM) and antimycin A (1 uM), and oxygen consumption rates (OCR) were quantified. For glycolysis stress tests, 300,000 cells/well were suspended in Seahorse XF RPMI medium with 2 mM L-glutamine; cells were treated serially with glucose (25 mM), oligomycin (5 μM), and 2-DG (100 mM), and extracellular acidification rates (ECAR) were measured over time. Cell numbers at assay completion were normalized to DNA content using CyQuant dye (Thermo Fischer Scientific, #C7026). Wave, Excel, and Graph Pad Prism software were used to analyze and graph the data.

Western blot analysis:

Splenocyte extracts were prepared using Pierce RIPA Buffer (Thermo Fisher, #8990) with protease and phosphatase cocktail inhibitors. Protein concentration was determined using BCA Protein Assay Reagent (Pierce, #23227, Rockford, IL). Protein was resolved on NuPAGE 4–12% Bis-Tris gel, transferred to a nitrocellulose membrane, then blocked for 1 h with 10 % BSA. Anti-mitochondrial antiviral signaling protein (MAVS) (SCTB, #sc-365334, Dallas, TX) was diluted 1:000 in 5% BSA, added and incubated overnight at 4°C. Monoclonal antibody against GAPDH (Invitrogen, #MA1–16757) was used as loading control and incubated for 1 hour at room temperature. After incubation with primary antibodies, membranes were washed three times and incubated with secondary antibodies coupled to IRDye 800CW. Membranes were developed using Li-COR Odyssey Clx scanner (Li-COR, Lincoln, NE).

Isolation of human primary derived macrophage and cytokine measurements:

Subjects gave informed consent to participate in an NIH-IRB approved protocol (94-AR-0066). Human PBMCs were obtained by Ficoll density gradient (Lymphoprep™, #07801, Stemcell Technologies, Cambridge, MA) of whole blood from healthy donors or lupus patients. $CD14^+$ monocytes were purified by positive selection using magnetic separation systems (MACS, #130–050-201, Miltenyi Biotec, Auburn, CA). Cells were cultured at 0.5×10^6 cells/ml during six days in RPMI 1640 medium (Gibco, #11875093, Thermo Fisher,) with 10 % FBS containing GM-CSF 25 ng/mL (Peprotech, #300–03, East Windsor, NJ) or M-CSF 10 ng/mL (R&D Systems, c#216-MC) to generate GM-macrophages and M-macrophages, respectively. Cytokines were replaced every two days.

Six-day cultured macrophages were preincubated with 4-OI (0.5 mM or 1.0 mM) for 3 hours and then cultured in the presence or absence of 100 ng/ml *E. coli* 0111:B4 LPS (SIGMA-Aldrich #L2630) for 24 h. Macrophage supernatants were harvested and stored at −80°C until tested by ELISA (BD Biosciences) to quantify secreted human TNF-α (#555212), IL-6 (#555220), IL-10 (#555157), IL-1β (#557953) and IL-8 (#555244).

Isolation, culture, and stimulation of B cells:

Healthy control PBMCs were isolated with Ficoll gradient and treated with MojoSort Human Pan B Cell Isolation Kit (BioLegend, #480081). $CD19^+$ B cell purity was above 90%. Purified $CD19^+$ B cells (50,000 cells/ 200 ul) were cultured alone or with 1000 U/ml IFN-alpha (Abcam # ab285741), 0.5 uM CpG-ODN (Invivogen, #tlrl-2216, San Diego, CA), or 1 ug/ml anti-IgM BCR (Jackson ImmunoResearch, #109–006-129, West Groove, PA)

in 96-well plates. The 4-OI (1 uM) and glutathione ethyl ester GSH-EE 0.5 uM (Cayman Chemical, catalog 14953) were added at day 0 and remained in the culture for the duration of the assay. Culture medium was RPMI 1640 supplemented with 10% FCS, 100 U/ml penicillin, and 100 U/ml streptomycin.

B cell proliferation analysis:

B cells were stained with BD Horizon™ CFSE 1 uM (BD Biosciences, #565082) following manufacturer's instructions. Cells were washed twice and cultured (5 days for the first two donors and 7 days for the third donor). Analysis was performed using an Attune NxT Flow Cytometer, then using the FlowJo™ software and the proliferation modeling tool to get the percentage of divided B cells.

IgG ELISA:

For quantification of *in vitro* IgG secretion, B cells were cultured alone or with *in vitro* stimulation in 96-well plates as described above. IgG levels in the medium were determined with a Total Human IgG ELISA kit (Thermo Scientific, #88-50550-22) following manufacturer's instructions.

Statistical analysis:

Statistical analysis was done using GraphPad Prism software.

Results

Lupus nephritis severity and autoantibodies decrease with 4-OI treatment.

Use of 4-OI led to histopathologic improvements of severity, inflammation, and global scores when compared with vehicle-treated mice (Figures 1A–B). Morphologically, there was noticeable kidney histology improvement upon treatment with 4-OI. Specifically, in the 4-OI treated group, kidneys showed remarkable reduced inflammation (arrowheads in Figure 1A, H&E) compared with vehicle-treated group. In addition, glomerulosclerosis (arrows in Figure 1A, PAS) and fibrosis were also less severe in 4-OI treated group. The total renal severity score was lower in 4-OI treated mice than in vehicle treated (Figure 1B). Furthermore, IC deposition was significantly reduced in the 4-OI group compared to vehicle alone (Figures 2A–B). These histologic changes were associated with decreases in albumin:creatinine ratio in the 4-OI group (Figure 2C), compared to the vehicle group, indicating improvement in kidney function. One of the mice in the 4-OI treatment spontaneously succumbed at day 26 from kidney failure.

Serum autoantibodies against RNP were significantly decreased while anti-ds-DNA also decreased, albeit not significantly, in the 4-OI group, when compared to the vehicle group (Figures 2D–E). Supporting these findings, *in vitro* incubation of human B cells with 4-OI inhibited proliferation and total IgG secretion, even in the presence of the GSH-EE cell permeant glutathione compound that prevents 4-OI protein alkylation (Figures 2F–G). Overall, *in vivo* 4-OI treatment led to improvement of murine lupus glomerulonephritis and decreased *in vivo* autoantibody levels, while *in vitro* 4-OI decreased human B cell proliferation and IgG synthesis.

Use of 4-OI improves thrombocytopenia and modulates lymphoid organ responses in murine lupus.

Body weight remained similar between the two treatment groups, while spleen:body weight ratio in 4-OI treated mice was significantly reduced compared to vehicle alone (Figure 3A). A recent report has indicated that 4-OI can inhibit JAK1 kinase activity (28). Supporting these findings, JAK1 activation (ratio of phospho/total-JAK1) in murine lupus splenocytes was significantly reduced in the *in vivo*-treated 4-OI group compared to vehicle alone (Figure 3B).

NZB/W mice develop thrombocytopenia and vascular dysfunction as part of immune mediated dysregulation. Mice treated with 4-OI had significant improvements in platelet counts (Figure 3C) and endothelium-dependent vasorelaxation (supplementary Figure 1S) when compared to vehicle treatment.

Splenocyte gene expression analysis revealed significant decreases in *Ifna*, *Ifnb*, *Il6*, *Il1b* and *Tnf* with 4-OI treatment compared to vehicle (Figure 4A). As itaconic acid is a mitochondrial immune-metabolite that reduces oxidative stress, we quantified *16s* gene expression as a surrogate of mitochondrial transcription and found it significantly increased with 4-OI group compared to vehicle (Figure 4B), suggesting a beneficial effect in mitochondrial physiology. With regards to immune cell composition in spleen, 4-OI effects were mild and included significant increases in the mean fluorescent intensity of CD80, but not CD86, in DCs and B cells (Supplementary Figure 2S). The percentage of splenic CD8 T cells was significantly increased by 4-OI compared to vehicle, with a significant reduction in the CD4:CD8 ratio (4.1 ± 0.6 vehicle versus 2.6 ± 0.2 4-OI; $p<0.03$, Student's t-test). As a surrogate for assessing Tregs, we quantified splenocyte gene expression of cytokine associated genes and Treg differentiation gene markers. Gene transcription of transcription factor Helios (*Ikzf2*) and components of suppressive cytokines *Ebi3* (Il35) and *p40* (29) were significantly enhanced, supporting that 4-OI induces immunoregulatory effects (Figure 4C).

MAVS is an essential adaptor for RIG-I/MDA5 signaling and sensing of RNA; it plays pathogenic roles in some murine lupus models. Because MAVS forms oligomers in lupus cells in high oxidative stress conditions (30), we measured MAVS protein expression by Western blot. MAVS monomers and oligomers were decreased in the 4-OI group compared to vehicle (Figure 4D). Overall, these results indicate that 4-OI attenuates oxidative damage and immune dysregulation in lymphoid organs in murine lupus.

4-OI modulates neutrophil responses.

Neutrophils contribute to oxidative stress during inflammatory responses. To analyze the effect of 4-OI in neutrophil phenotype and function, we tested the ability of BM-derived-neutrophils to form NETs, a feature that is dysregulated in murine and human lupus in association with aberrant mROS synthesis (23). Mice treated with 4-OI showed a trend for enhanced basal NET formation and mROS synthesis; however, they displayed unresponsiveness to calcium ionophore-induced NET formation and enhanced mROS

(Figures 5A–B). These data suggest that 4-OI attenuates neutrophil activation and NET formation in response to stimulation.

As the itaconate pathway is involved in the regulation of metabolism, we analyzed the effect of 4-OI in the bioenergetics of BM-derived macrophages and splenocytes. While oxidative phosphorylation (OXPHOS) was not significantly modulated in macrophages after *in vivo* 4-OI administration, glycolysis was significantly inhibited (Figure 5C). Splenocytes, which in lupus have been described to exhibit enhanced mitochondrial OXPHOS (31), displayed significant OXPHOS reduction after 4-OI exposure when compared to vehicle treated mice (Figures 5D–E), including reductions in basal and maximal respiration, proton leak, and ATP production. Overall, 4-OI modulated immune-metabolic parameters in murine lupus.

In vitro 4-OI modulates inflammatory responses in human myeloid cells.

To further assess the effects of 4-OI in human lupus, we quantified if it could modulate proinflammatory responses of human monocyte-derived macrophages and NET formation in human neutrophils. Healthy control or SLE peripheral blood monocytes were differentiated into GM (M1, proinflammatory) or M (M2, anti-inflammatory) macrophages, treated with 4-OI, stimulated with 100 ng/ml LPS for 24 h, and cytokine secretion was quantified. *In vitro*, both 0.5 or 1 uM 4-OI concentrations significantly reduced the levels of secreted IL1-beta, IL6, TNF, and IL-10, particularly in the GM macrophages (Figures 6A–D). Furthermore, 4-OI inhibited secretion of IL1-beta and IL-10 by healthy control macrophages (Figures 6A, and 6D). In contrast, there was no modulation of IL-8 secretion by 4-OI in control or SLE-derived macrophages (Figure 6E). Additionally, NET formation by healthy control or SLE neutrophils was inhibited with 1 uM 4-OI (Figures 6F–H). These data support an immunoregulatory role of 4-OI on human myeloid cells.

Discussion

We found that subcutaneous administration of 4-OI improves features of murine lupus when treatment is initiated once clinical disease is already established. The beneficial effects were observed in renal function, histopathology and IC deposition, platelet counts, vascular dysfunction and in the levels of circulating autoantibodies. Furthermore, the drug inhibited inflammatory responses in immune cells and changed immune-metabolic parameters. These effects might be related with the already documented ability of itaconate to attenuate proinflammatory pathways in other inflammatory models. Given that most immune cells subsets in lymphoid organs did not significantly change, it remains to be further determined the mechanisms by which autoimmune responses were hampered in murine lupus, but it could be related to modulation of myeloid cell dysregulation with downstream effects on other innate and adaptive immune cells, including Tregs and B cells.

Levels of various antinuclear antibodies as well as type I IFN pathway dysregulation were reduced by 4-OI administration. The mechanisms leading to downmodulation of these autoimmune responses are likely multifactorial. As autoantigen/autoantibody ICs can trigger type I IFN production (32), it is possible that modulation of IC formation, through 4-OI decreasing autoantigen generation by inhibiting NET formation or other types of inflammatory cell death, may decrease immune dysregulation. Decreases in synthesis and

release of other inflammatory cytokines by immune cells observed with 4-OI may also hamper autoantibody generation, as previously reported (33, 34). Among the effect that 4-OI had on various cytokines, it reduced the ability of human macrophages to secrete IL-10. This cytokine may play pathogenic roles in SLE, including autoantibody synthesis (35–37). It is therefore possible that decreases in autoantibodies and improvement in platelet numbers following 4-OI treatment could be due in part to effects on IL-10 synthesis, besides the direct inhibition of B cell function that was observed by *in vitro* human studies. Given that inhibition of B cell proliferation and IgG secretion by human B cells after 4-OI treatment was not alkylation-dependent, it is possible that the immunomodulation might be through other effects in immunometabolism such as inhibition of succinate dehydrogenase (38), which should be explored in future studies.

Recently described attenuation of specific allergic inflammatory responses in mice by 4-OI intranasal treatment was accomplished via reduction of DC priming activity (39). A similar phenomenon might take effect here, where 4-OI treatment could partially reduce DC priming responses to lupus autoantigens. Other possible effects of 4-OI to explain the elevated numbers of CD8+ T cells in 4-OI- treated animals is by the observed inhibition of glycolysis and mTOR pathways. This is supported by previous findings that rapamycin, an inhibitor of mTOR, can increase both CD8 T cells and Treg function in SLE patients with concomitant improvement in disease activity (40, 41). While FOXP3 levels were not transcriptionally regulated by treatment, future studies should assess whether survival of memory CD8 T cells and CD8-specific FOXP3 expression or Treg suppressor function are affected by this treatment. Another important aspect is the regulation of perturbed metabolic responses with 4-OI. Proinflammatory macrophages (M1) rely on glycolysis and exhibit impairment of the TCA cycle and OXPHOS, whereas anti-inflammatory macrophages (M2) are more dependent on mitochondrial OXPHOS (42). In our study, 4-OI treatment attenuated glycolysis in BM-derived macrophages, and this may have significant relevance in lupus-prone mice, as enhanced glycolysis is associated with the elevated proinflammatory environment characteristic of SLE. Indeed, blunting glycolysis in macrophages has been reported to improve lupus nephritis in mice (43). In addition, 4-OI treatment enhanced the mitochondrial gene transcription, suggesting a potential improvement in mitochondrial function (24, 44). Furthermore, the reduction of MAVS oligomerization with 4-OI suggests that the oxidative stress status was reduced, most probably through the NRF2 pathway, given that ROS play a role in inducing MAVS-dependent responses in SLE (30). This in turn may help decrease aberrant responses to nucleic acids in lupus cells. In addition, 4-OI promoted decreased ability of murine and human neutrophils to synthesize NETs.

Part of the mechanism that may be involved in blunting inflammatory responses is through the recently described role of 4-OI in modulating JAK1-mediated pathways. The JAK/STAT pathway plays fundamental roles in SLE (45). We observed that 4-OI blunted activation of JAK1 in murine lupus as recently described (28). Overall, these results indicate that 4-OI exerts pleiotropic anti-inflammatory effects on myeloid cells and adaptive immune cells.

Limitations of the study include the use of a single mouse model of lupus and that effects on other potential lupus manifestations (such as skin involvement) were therefore not addressed. It is important to mention that the beneficial effects were observed when therapy

was started only after immune dysregulation and organ damage were well established. Serum concentrations of itaconic acid have been previously reported to be significantly reduced in SLE patients with active disease, when compared to healthy controls (46). As we observed amelioration of established murine lupus, our results add new evidence to the existing literature that suggests that modulation of immunometabolism may be a viable therapeutic strategy in SLE and other systemic autoimmune disorders. This was supported by the beneficial effects observed in human cells *in vitro*. These results support the possibility of further exploring the role of itaconate-derived medications in autoimmune disorders such as SLE.

Supplementary Material

Refer to Web version on PubMed Central for supplementary material.

Acknowledgments

We thank the Office of Science and Technology, Intramural Research Program, NIAMS/NIH for technical support. This study was supported by the Intramural Research Program, NIAMS/NIH (ZIA AR041199). HLP was supported by the Northern Norway Regional Health Authority grant HNF1343-17.

Funding:

Supported by the Intramural Research Program at NIAMS/NIH (ZIA AR041199 03-05). HLP was supported by a Northern Norway Regional Health Authority grant (HNF1343-17).

Literature cited.

1. Kaplan MJ. Role of neutrophils in systemic autoimmune diseases. Arthritis Research & Therapy. 2013;15(5):219-. [PubMed: 24286137]
2. Mohan C, Putterman C. Genetics and pathogenesis of systemic lupus erythematosus and lupus nephritis. Nat Rev Nephrol. 2015;11(6):329–41. [PubMed: 25825084]
3. Kiriakikidou M, Chin KL. Systemic Lupus Erythematosus. Annals of Internal Medicine. 2020;172(11):ITC81–ITC96. [PubMed: 32479157]
4. Crow MK, Olferiev M, Kirou KA. Type I Interferons in Autoimmune Disease. Annual Review of Pathology: Mechanisms of Disease. 2019;14(1):369–93.
5. Li Z, Guo J, Bi L. Role of the NLRP3 inflammasome in autoimmune diseases. Biomedicine & Pharmacotherapy. 2020;130:110542. [PubMed: 32738636]
6. Perl A. Oxidative stress in the pathology and treatment of systemic lupus erythematosus. Nat Rev Rheumatol. 2013;9(11):674–86. [PubMed: 24100461]
7. Lightfoot YL, Blanco LP, Kaplan MJ. Metabolic abnormalities and oxidative stress in lupus. Current Opinion in Rheumatology. 2017;29(5).
8. Romo-Tena J, Kaplan MJ. Immunometabolism in the pathogenesis of systemic lupus erythematosus: an update. Current Opinion in Rheumatology. 2020;32(6).
9. Kim J, Gupta R, Blanco LP, Yang S, Shteinfer-Kuzmine A, Wang K, et al. VDAC oligomers form mitochondrial pores to release mtDNA fragments and promote lupus-like disease. Science. 2019;366(6472):1531–6. [PubMed: 31857488]
10. Hooftman A, O'Neill LAJ. The Immunomodulatory Potential of the Metabolite Itaconate. Trends in Immunology. 2019;40(8):687–98. [PubMed: 31178405]
11. Diskin C, Ryan TAJ, O'Neill LAJ. Modification of Proteins by Metabolites in Immunity. Immunity. 2021;54(1):19–31. [PubMed: 33220233]
12. Luan Harding H, Medzhitov R. Food Fight: Role of Itaconate and Other Metabolites in Antimicrobial Defense. Cell Metabolism. 2016;24(3):379–87. [PubMed: 27626199]

13. Mills EL, Ryan DG, Prag HA, Dikovskaya D, Menon D, Zaslona Z, et al. Itaconate is an anti-inflammatory metabolite that activates Nrf2 via alkylation of KEAP1. Nature. 2018;556(7699):113–7. [PubMed: 29590092]
14. Liao S-T, Han C, Xu D-Q, Fu X-W, Wang J-S, Kong L-Y. 4-Octyl itaconate inhibits aerobic glycolysis by targeting GAPDH to exert anti-inflammatory effects. Nature communications. 2019;10(1):5091-.
15. Olagnier D, Brandtoft AM, Gunderstofte C, Villadsen NL, Krapp C, Thielke AL, et al. Nrf2 negatively regulates STING indicating a link between antiviral sensing and metabolic reprogramming. Nature communications. 2018;9(1):3506-.
16. Li R, Yang W, Yin Y, Ma X, Zhang P, Tao K. 4-OI Attenuates Carbon Tetrachloride-Induced Hepatic Injury via Regulating Oxidative Stress and the Inflammatory Response. Frontiers in pharmacology. 2021;12:651444-.
17. Li Y, Chen X, Zhang H, Xiao J, Yang C, Chen W, et al. 4-Octyl Itaconate Alleviates Lipopolysaccharide-Induced Acute Lung Injury in Mice by Inhibiting Oxidative Stress and Inflammation. Drug Des Devel Ther. 2020;14:5547–58.
18. Liu G, Wu Y, Jin S, Sun J, Wan B-B, Zhang J, et al. Itaconate ameliorates methicillin-resistant Staphylococcus aureus-induced acute lung injury through the Nrf2/ARE pathway. Ann Transl Med. 2021;9(8):712-. [PubMed: 33987410]
19. Tian F, Wang Z, He J, Zhang Z, Tan N. 4-Octyl itaconate protects against renal fibrosis via inhibiting TGF-β/Smad pathway, autophagy and reducing generation of reactive oxygen species. European Journal of Pharmacology. 2020;873:172989. [PubMed: 32032597]
20. Xin Y, Zou L, Lang S. 4-Octyl itaconate (4-OI) attenuates lipopolysaccharide-induced acute lung injury by suppressing PI3K/Akt/NF-κB signaling pathways in mice. Experimental and therapeutic medicine. 2021;21(2):141-. [PubMed: 33456508]
21. Li R, Yang W, Yin Y, Zhang P, Wang Y, Tao K. Protective Role of 4-Octyl Itaconate in Murine LPS/D-GalN-Induced Acute Liver Failure via Inhibiting Inflammation, Oxidative Stress, and Apoptosis. Oxidative Medicine and Cellular Longevity. 2021;2021:9932099.
22. Tang C, Wang X, Xie Y, Cai X, Yu N, Hu Y, et al. 4-Octyl Itaconate Activates Nrf2 Signaling to Inhibit Pro-Inflammatory Cytokine Production in Peripheral Blood Mononuclear Cells of Systemic Lupus Erythematosus Patients. Cellular Physiology and Biochemistry. 2018;51(2):979–90. [PubMed: 30466076]
23. Lood C, Blanco LP, Purmalek MM, Carmona-Rivera C, De Ravin SS, Smith CK, et al. Neutrophil extracellular traps enriched in oxidized mitochondrial DNA are interferogenic and contribute to lupus-like disease. Nature medicine. 2016;22(2):146–53.
24. Blanco LP, Pedersen HL, Wang X, Lightfoot YL, Seto N, Carmona-Rivera C, et al. Improved Mitochondrial Metabolism and Reduced Inflammation Following Attenuation of Murine Lupus With Coenzyme Q10 Analog Idebenone. Arthritis & Rheumatology. 2020;72(3):454–64. [PubMed: 31566908]
25. Carmona-Rivera C, Purmalek MM, Moore E, Waldman M, Walter PJ, Garraffo HM, et al. A role for muscarinic receptors in neutrophil extracellular trap formation and levamisole-induced autoimmunity. JCI Insight. 2017;2(3):e89780. [PubMed: 28194438]
26. Furumoto Y, Smith CK, Blanco L, Zhao W, Brooks SR, Thacker SG, et al. Tofacitinib Ameliorates Murine Lupus and Its Associated Vascular Dysfunction. Arthritis & Rheumatology. 2017;69(1):148–60.
27. Gupta S, Nakabo S, Blanco LP, O'Neil LJ, Wigerblad G, Goel RR, et al. Sex differences in neutrophil biology modulate response to type I interferons and immunometabolism. Proceedings of the National Academy of Sciences. 2020;117(28):16481–91.
28. Runtsch MC, Angiari S, Hooftman A, Wadhwa R, Zhang Y, Zheng Y, et al. Itaconate and itaconate derivatives target JAK1 to suppress alternative activation of macrophages. Cell Metab. 2022;34(3):487–501.e8. [PubMed: 35235776]
29. Lee S-Y, Moon S-J, Moon Y-M, Seo H-B, Ryu J-G, Lee AR, et al. A novel cytokine consisting of the p40 and EBI3 subunits suppresses experimental autoimmune arthritis via reciprocal regulation of Th17 and Treg cells. Cellular & Molecular Immunology. 2022;19(1):79–91. [PubMed: 34782759]

30. Buskiewicz IA, Montgomery T, Yasewicz EC, Huber SA, Murphy MP, Hartley RC, et al. Reactive oxygen species induce virus-independent MAVS oligomerization in systemic lupus erythematosus. Science Signaling. 2016;9(456):ra115-ra.

31. Wahl DR, Petersen B, Warner R, Richardson BC, Glick GD, Opipari AW. Characterization of the metabolic phenotype of chronically activated lymphocytes. Lupus. 2010;19(13):1492–501. [PubMed: 20647250]

32. Lövgren T, Eloranta M-L, Båve U, Alm GV, Rönnblom L. Induction of interferon-α production in plasmacytoid dendritic cells by immune complexes containing nucleic acid released by necrotic or late apoptotic cells and lupus IgG. Arthritis & Rheumatism. 2004;50(6):1861–72. [PubMed: 15188363]

33. Dienz O, Eaton SM, Bond JP, Neveu W, Moquin D, Noubade R, et al. The induction of antibody production by IL-6 is indirectly mediated by IL-21 produced by CD4+ T cells. Journal of Experimental Medicine. 2009;206(1):69–78. [PubMed: 19139170]

34. Nakae S, Asano M, Horai R, Iwakura Y. Interleukin-1 beta, but not interleukin-1 alpha, is required for T-cell-dependent antibody production. Immunology. 2001;104(4):402–9. [PubMed: 11899425]

35. Baglaenko Y, Manion KP, Chang N-H, Gracey E, Loh C, Wither JE. IL-10 Production Is Critical for Sustaining the Expansion of CD5+ B and NKT Cells and Restraining Autoantibody Production in Congenic Lupus-Prone Mice. PLOS ONE. 2016;11(3):e0150515.

36. Teichmann LL, Kashgarian M, Weaver CT, Roers A, Müller W, Shlomchik MJ. B cell-derived IL-10 does not regulate spontaneous systemic autoimmunity in MRL.Fas(lpr) mice. Journal of immunology (Baltimore, Md : 1950). 2012;188(2):678–85. [PubMed: 22156495]

37. Xu L, Wang L, Shi Y, Deng Y, Oates JC, Kamen DL, et al. Upregulated IL-10 induced by E2F2-miR-17–5p circuitry in extrafollicular effector B cells contributes to autoantibody production in systemic lupus erythematosus. Arthritis & Rheumatology. 2021;n/a(n/a).

38. Domínguez-Andrés J, Novakovic B, Li Y, Scicluna BP, Gresnigt MS, Arts RJW, et al. The Itaconate Pathway Is a Central Regulatory Node Linking Innate Immune Tolerance and Trained Immunity. Cell Metabolism. 2019;29(1):211–20.e5. [PubMed: 30293776]

39. Jaiswal AK, Yadav J, Makhija S, Mazumder S, Mitra AK, Suryawanshi A, et al. Irg1/itaconate metabolic pathway is a crucial determinant of dendritic cells immune-priming function and contributes to resolute allergen-induced airway inflammation. Mucosal Immunology. 2021.

40. Lai Z-W, Kelly R, Winans T, Marchena I, Shadakshari A, Yu J, et al. Sirolimus in patients with clinically active systemic lupus erythematosus resistant to, or intolerant of, conventional medications: a single-arm, open-label, phase 1/2 trial. The Lancet. 2018;391(10126):1186–96.

41. Kato H, Perl A. Blockade of Treg Cell Differentiation and Function by the Interleukin-21–Mechanistic Target of Rapamycin Axis Via Suppression of Autophagy in Patients With Systemic Lupus Erythematosus. Arthritis & Rheumatology. 2018;70(3):427–38. [PubMed: 29161463]

42. Viola A, Munari F, Sánchez-Rodríguez R, Scolaro T, Castegna A. The Metabolic Signature of Macrophage Responses. Frontiers in Immunology. 2019;10(1462).

43. Jing C, Castro-Dopico T, Richoz N, Tuong ZK, Ferdinand JR, Lok LSC, et al. Macrophage metabolic reprogramming presents a therapeutic target in lupus nephritis. Proceedings of the National Academy of Sciences. 2020;117(26):15160–71.

44. Reyes A, Rusecka J, Tońska K, Zeviani M. RNase H1 Regulates Mitochondrial Transcription and Translation via the Degradation of 7S RNA. Frontiers in Genetics. 2020;10(1393).

45. Hedrich CM, Rauen T, Apostolidis SA, Grammatikos AP, Rodriguez Rodriguez N, Ioannidis C, et al. Stat3 promotes IL-10 expression in lupus T cells through trans-activation and chromatin remodeling. Proceedings of the National Academy of Sciences. 2014;111(37):13457–62.

46. Li Y, Liang L, Deng X, Zhong L. Lipidomic and metabolomic profiling reveals novel candidate biomarkers in active systemic lupus erythematosus. Int J Clin Exp Pathol. 2019;12(3):857–66. [PubMed: 31933894]

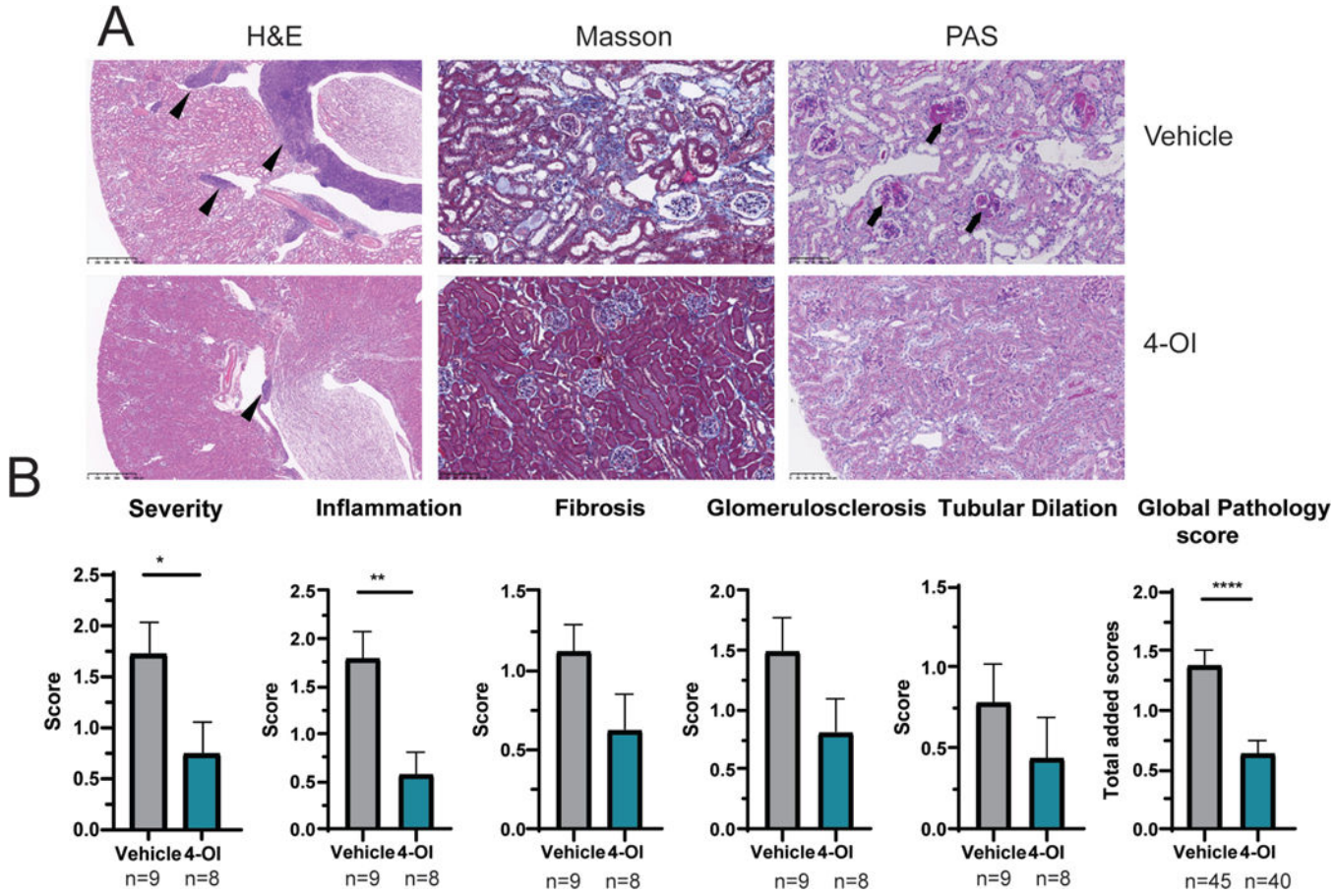

Figure 1: Attenuation of lupus kidney pathology by 4-OI.

A) Representative kidney tissue images showing H&E, Masson, and PAS staining. Magnifications are 40x for H&E and 200x for Masson and PAS. In H&E; arrowheads show inflammation. In PAS, arrows indicate glomerulosclerosis. **B)** Graphs display kidney pathology scores. Bar graphs represent mean ± SEM. In all studies mice were treated with 4-OI or vehicle control; n=number of animals except in global pathology score where all the individual scores (severity, inflammation, fibrosis, glomerulosclerosis, and tubular dilation) are graphed together per group. The statistical analysis was done using Mann Whitney test *:p<0.05, **:p<0.01: ****:p<0.001.

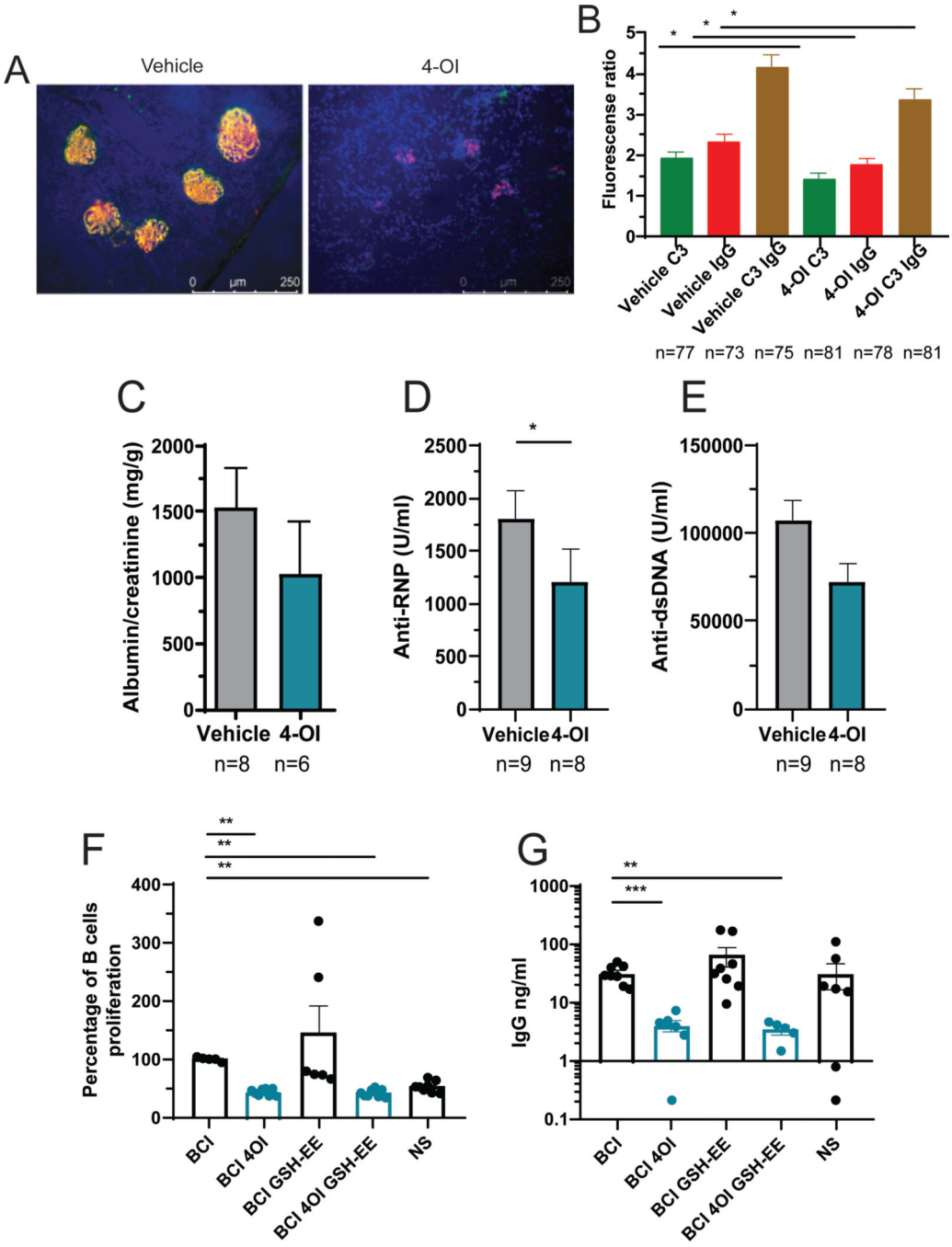

Figure 2: Attenuation of kidney damage, serum autoantibody levels, and human B cell responses by 4-OI.

A) Representative immunofluorescence microphotographs displaying IC deposition (IgG red, C3 green, nuclei in blue); magnification 40x. **B)** Image J quantification depicting pixel analysis of glomeruli in 3 different images/mouse from panel A. **C)** Analysis of proteinuria at the time of euthanasia. Serum antibodies against **D)** RNP, and **E)** ds-DNA; mice were treated with 4-OI or vehicle control with n numbers indicated in the figure; the discrepancy in numbers is due to failure to collect urine in some of the mice in C. **F)** Human B cell

proliferation after stimulation (BCI) or non-stimulation (NS) and **G)** total IgG secretion in 3 different healthy donors. Bar graphs represent mean ± SEM. The statistical analysis was done using Mann Whitney test *:$p<0.05$, **:$p<0.01$, ***:$p<0.001$.

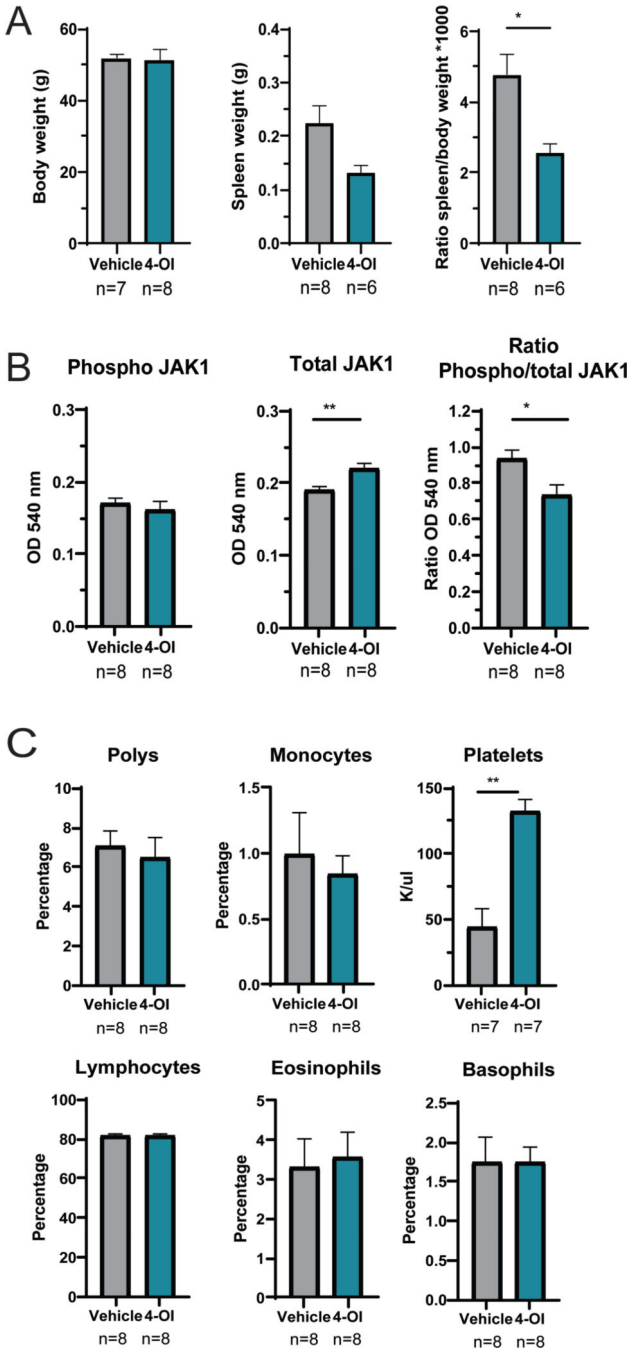

Figure 3: 4-OI modulates splenomegaly, JAK1 activation, and platelet counts.

A) Body and spleen weights, and their ratio are displayed. **B)** Spleen tissue was homogenized and phospho- and total- JAK1 protein were detected by ELISA. **C)** Complete blood counts. In both studies mice treated with 4-OI or vehicle control with n= numbers indicated in the figure; bar graphs represent mean ± SEM, and statistical analysis was done using Mann Whitney test *:$p<0.05$; **:$p<0.01$; outlier data points were detected using GraphPad ROUT method (Q=10%) and excluded from the analysis.

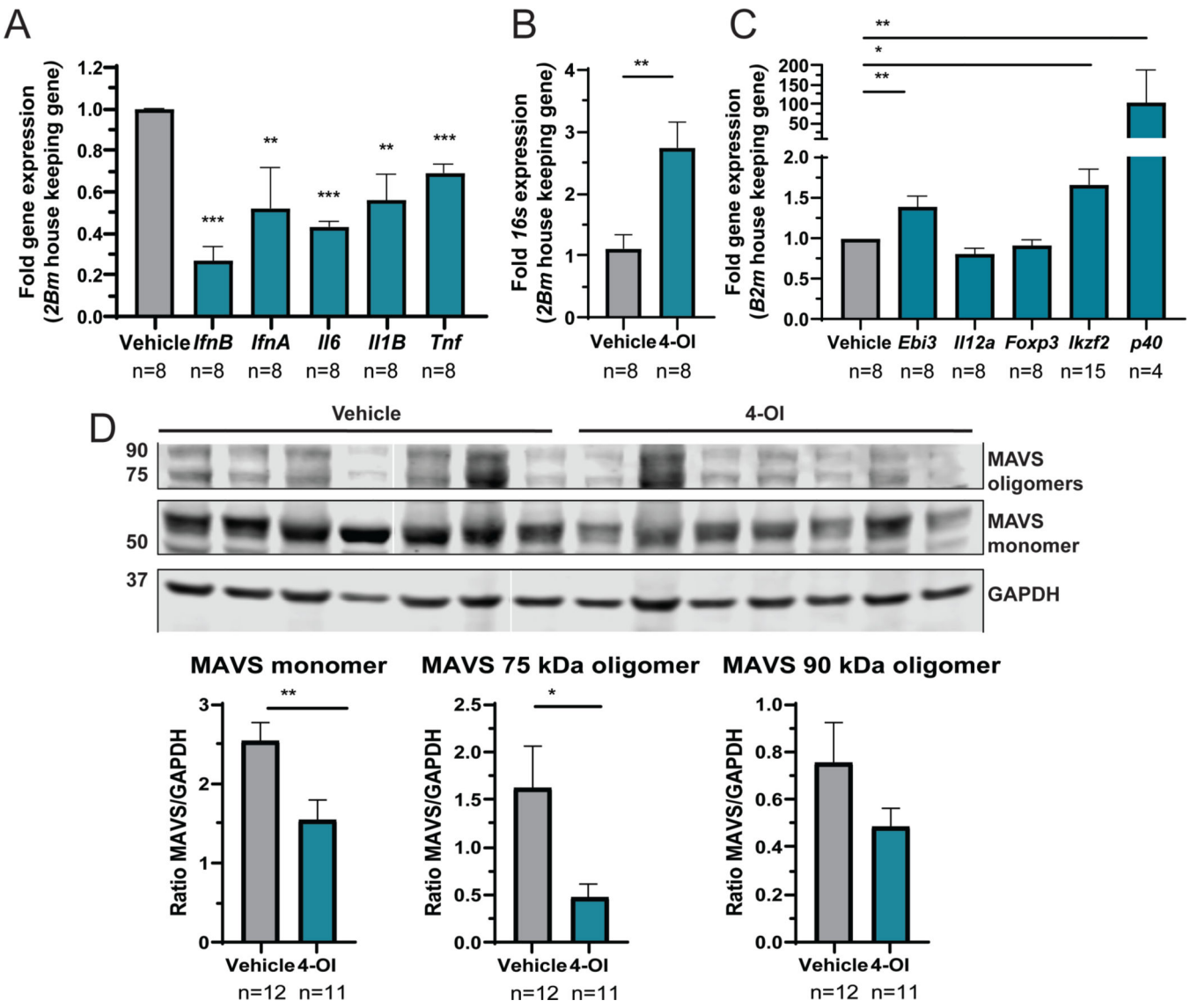

Figure 4: Effect of 4-OI in gene expression and inflammasome protein expression in spleen cells.

A) Gene expression in splenocytes was analyzed by q-RT-PCR normalized against *B2m* housekeeping gene. **B)** The *16s* mitochondrial gene expression in splenocytes was determined as a surrogate of mitochondrial transcriptional activity by q-RT-PCR. **C)** Gene expression of associated Treg markers. In these studies, mice were treated with 4-OI or vehicle control with n= numbers indicated in the figure corresponding to 4 animals per group and 2 technical duplicates, except for *Ikzf2* done in quadruplicate; the missing values are samples with no amplification. Statistical analysis was done using Mann Whitney test, **:p<0.01; ***:p<0.005. **D)** The expression of MAVS monomer, 75, and 90 kDA oligomers, and GAPDH wasquantified by Western blot in lysates of splenocytes from vehicle- or 4-OI-treated mice. Representative Western blot image of 2 similar experiments: the first blot was performed with 5 vehicle-treated animals and four 4-OI treated-animals; the second blot was with 7 animals in each group. Results represent the average ± SEM of protein

versus GAPDH loading control ratio. Statistical analysis was done using Mann Whitney test *:$p<0.05$; **:$p<0.01$.

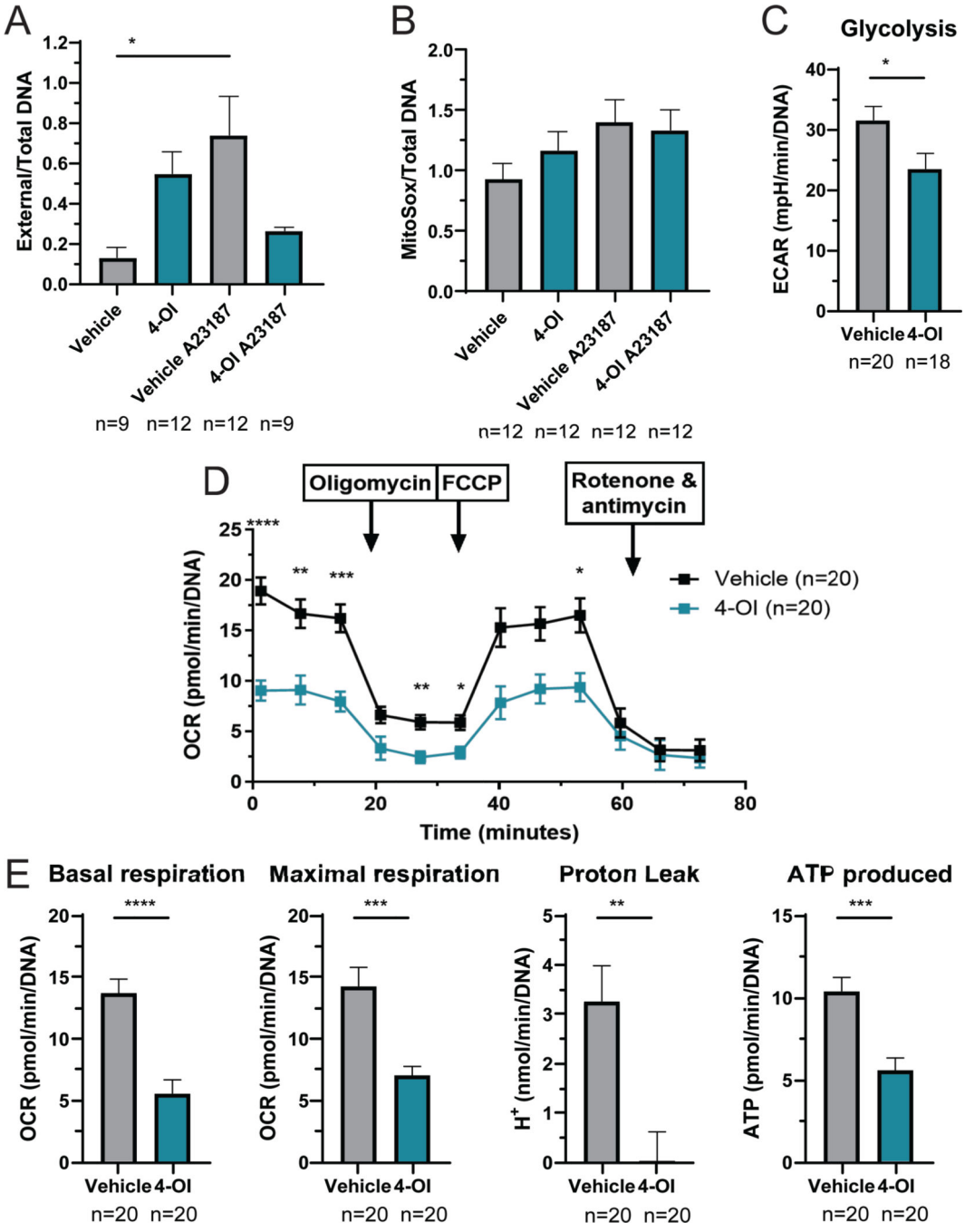

Figure 5: 4-OI modulates NET formation and immune-metabolism.

A) NETs were quantified in BM-derived neutrophils, 2 h post-plating, by SYTOX/Pico Green plate assay to measure external and total DNA, respectively. **B)** mROS was quantified in BM-derived neutrophils at 1 h using MitoSox, by plate assay. In both **A** and **B,** mice were treated with 4-OI or vehicle control per group; data points include 4 animals per group and 3 technical repeats, and neutrophils were stimulated with the A23187 calcium ionophore (250 uM) to induce NETs and mROS. The statistical analysis was done using Mann Whitney test *:p<0.05. **C)** Glycolysis of murine BM-differentiated macrophages, measured

by Seahorse; data points are shown which include 4 animals per group and 5 technical repeats. **D)** Seahorse mitochondrial stress test analysis of splenocytes; statistical analysis using 2-way ANOVA. **E)** Parameters for splenocytes calculated from **D**. Seahorse studies included mice treated with 4-OI or vehicle control per group; data points shown include 4 animals per group and 5 technical repeats. Bar graphs represent mean ± SEM. The statistical analysis was done using Mann Whitney test, **:$p<0.01$; ***:$p<0.005$; ****$p<0.001$. In these experiments outlier data points excluded were detected using GraphPad ROUT method (Q=10%).

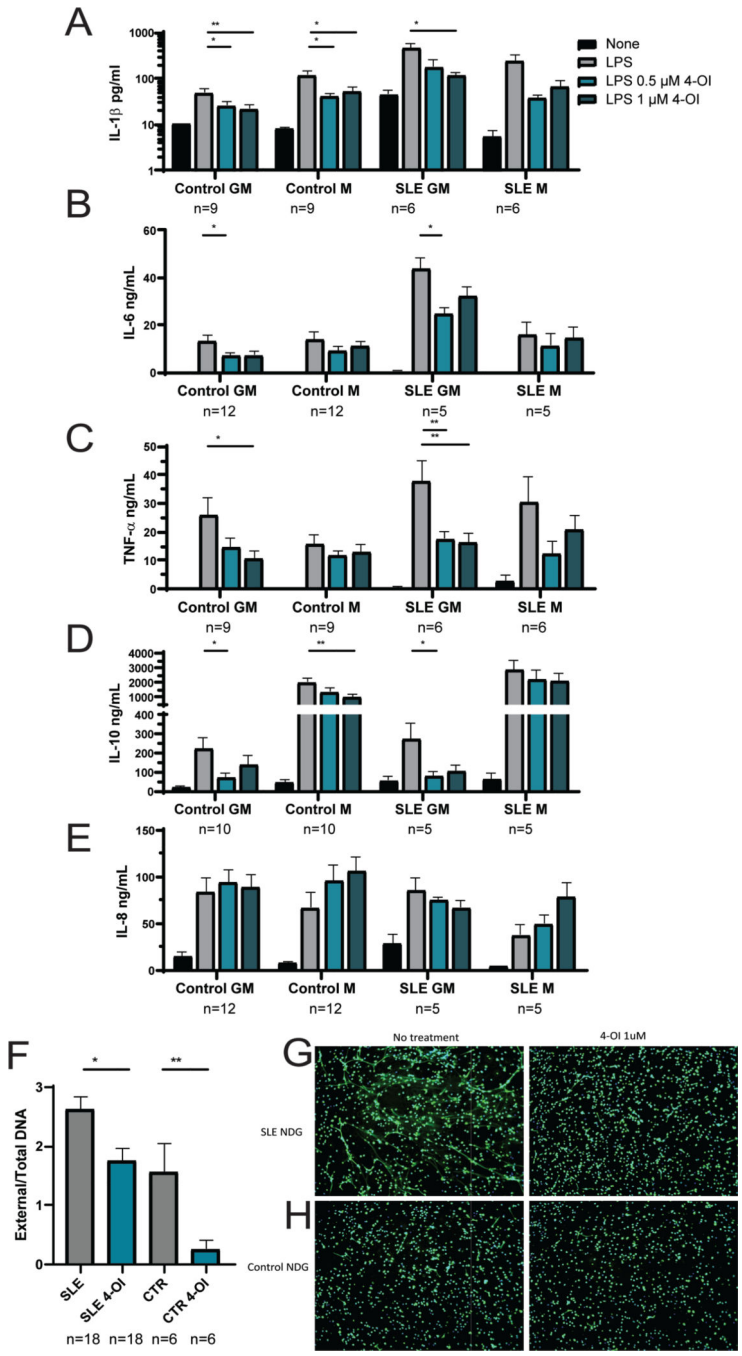

Figure 6: *In vitro* effect of 4-OI on cytokine release by human-monocyte derived primary macrophages and NET formation by human neutrophils.

A-E) Human primary monocyte-derived macrophages (at least n=6 from different donors) were obtained from healthy control or SLE subjects circulating monocytes by differentiating with either GM-CSF (GM proinflammatory) or M-CSF (M anti-inflammatory) for 7 days. Cytokines in supernatants were measured by ELISA after 24 h treatment with 4-OI or vehicle. The cytokines measured were **A)** IL1-beta, **B)** IL-6, **C)** TNF-alpha, **D)** IL-10, and **E)** IL-8. **F)** NET formation in normal dense granulocytes (NDGs) measured by fluorometry

plate assay. Shown is mean ± SEM from SLE and healthy control (CTR) neutrophils, with numbers indicated in the figure, corresponding to 9 SLE and 3 healthy controls, done by technical duplicates; **G-H)** and by fluorescent microscopy imaging showing merged immunofluorescence staining with primary antibody against neutrophil elastase (green) and DNA (nuclei and NET fibers, Hoechst, blue); representative images of neutrophils from G) SLE and from H) healthy controls; magnification is 10 x. Bar graphs represent mean ± SEM. The statistical analysis was done using Mann Whitney test *:$p<0.05$; **:$p<0.01$